EUROPEAN FUSION DEVELOPMENT AGREEMENT

EFDA–JET–PR(03)14

C. P. Perez, H. R. Koslowski, P. Smeulders, G. T. A. Huysmans, S. Jachmich,
T. Eich, A. Loarte, G. Saibene, T. C. Hender, R. J. Hastie, M. Becoulet,
P. J. Lomas, R. Sartori, A. Rogister, F. C. Schueller
and JET EFDA contributors

Washboard Modes as ELM-related Events in JET

Washboard Modes as ELM-related Events in JET

C. P. Perez[1], H. R. Koslowski[1], P. Smeulders[2], G.T.A. Huysmans[3], S.Jachmich[1], T.Eich[4], A.Loarte[5], G.Saibene[5], T.C. Hender[6], R.J. Hastie[6], M. Becoulet[3], P. J. Lomas[6], R. Sartori[5], A. Rogister[1], F. C. Schueller[7]
and JET EFDA contributors*

[1]Association EURATOM-Forschungszentrum Jülich, Institut fÄ ur Plasmaphysik, Trilateral Euregio Cluster, D-52425 Jülich, Germany
[2]Associazione EURATOM-ENEA sulla Fusione, Centro Ricerche Frascati, C.P. 65, 00044-Frascati (Rome), Italy
[3]Association EURATOM-CEA, Cadarache, F-13108 St. Paul-lez-Durance, France
[4]Max-Planck-Institut für Plasmaphysik, EURATOM Assoziation, Garching D-85748, Germany
[5]EFDA-CSU, Max-Planck-Institut fÄ ur Plasmaphysik, Garching D-85748, Germany
[6]EURATOM/UKAEA Fusion Association, Culham Science Centre, Abingdon, OX14 3DB, UK
[7]FOM-Rijnhuizen, Ass. EURATOM-FOM, TEC, PO Box 1207, 3430 BE Nieuwegein, NL
** See annex of J. Pamela et al, "Overview of Recent JET Results and Future Perspectives", Fusion Energy 2000 (Proc. 18th Int. Conf. Sorrento, 2000), IAEA, Vienna (2001).*

Preprint of Paper to be submitted for publication in
Plasma Physics and Controlled Fusion

ABSTRACT.
Washboard (WB) modes are a very regular phenomenon commonly observed in JET H-Mode discharges, appearing as broader bands of bursting magnetic fluctuation at the plasma edge. It will be shown that WB modes are deeply involved in the pedestal dynamics, affecting the pedestal build-up through inter-ELM losses. In close relation to this, the time between consecutive type-I ELMs increases with WB mode strength. A class of type-I ELM precursors commonly observed in JET [C P Perez et al, to be published in Nucl. Fusion] is found to interact with WB modes: With the onset of type-I ELM precursors the WB modes become weaker or are even inhibited, resulting in an acceleration of the pedestal pressure build-up. WB activity is found to increase with gas puffing at high triangularity, and can explain the recently identified mixed type-I/type-II ELM regime on JET. A modified version of the peeling-ballooning cycle for type-I ELMs, that takes into account the physics of WB modes, is proposed.

1. INTRODUCTION

The energy losses associated with type-I ELMs [1–3] are a serious concern for ITER due to the possibly unacceptable transient heat loads expected on the divertor tiles. The understanding of type-I ELMs, in particular their origin and the underlying processes governing their dynamics, is still incomplete. From the MHD point of view, research is increasingly focussing on the role of the most promising ideal instabilities, namely (finite-) ballooning and kink-(peeling) modes, and recently also on coupled ballooning-kink modes, leading to the proposition of a so called peeling-ballooning cycle for type-I ELMs [4].

Washboard (WB) modes are a very robust phenomenon commonly observed in JET H-Mode discharges, and are not thought to belong to one of the above mentioned instabilities. Since their discovery [5], rather little attention has been paid to them, either theoretically or experimentally. So far they have not been regarded as an ELM-relevant instability. However, in this paper evidence for their deep involvement in the pedestal and ELM dynamics will be presented.

The paper is organized as follows. In section 2 an overview of WB properties is given, recalling earlier findings from [5] where appropriate. The relationship between WB modes and the regime labeled as type-II ELM regime in JET is discussed in section 3, and the interaction of type-I ELM precursors with WB modes in section 4. Building on these findings, a modified version of the peeling-ballooning cycle for type-I ELMs that takes into account the physics of WB modes will be proposed in section 5. Finally, a summary and a discussion of the results are given.

2. WB PROPERTIES

Figure 1 shows a spectrum of toroidal mode numbers for an example ELMy H-Mode, where the colours denote the toroidal mode numbers n. The n-numbers are obtained by making a time-windowed Fourier decomposition of the signals of a toroidal set of Mirnov coils and analysing the relative phase shift of the fluctuations. The procedure is described in more detail in [6]. Toroidal

mode number spectra are convenient for discriminating the various types of MHD activity present (in particular the WB modes) and will be often used throughout this paper. Positive and negative mode numbers are detected. Modes with negative n rotate in the opposite direction to modes with positive n. The convention n used here is that modes with negative rotate in the direction of the electron diamagnetic drift. Three type-I ELMs occur at 22.096s, 22.24s and 22.36s. In between them one can observe several blue coloured broader bands with frequencies ranging from ~10-80kHz propagating in the direction of the electron-diamagnetic drift. These are the WB modes. They have a quite characteristic frequency evolution in between ELMs. When WB modes reappear after an ELM both the WB frequency and the spectral extent are initially low, but then gradually increase until the next ELM occurs. WB modes typically have mode numbers in the range $n = -1$ to -8. In addition, the red coloured modes (n = +8) aroun 20kHz are type-I eLM precursors, whose properties were presented elsewhere [6]. We shall come back to them later.

WB modes are located at the plasma edge. Figure 2 shows previous results of a coherence analysis for a hot-ion H-Mode discharge [7] with particularly prominent WB modes. The coherence analysis uses a reference Mirnov signal and channels of the JET edge reflectometer with cut-off densities ranging from 0.43 to 4.13×10^{19} m^{-3}. The upper plots give the values of the coherence and phase of the cross-spectral density, respectively, as a function of major radius R and frequency f. The dashed lines denote the measuring radii of the reflectometer channels estimated on the basis of a density profile obtained by the core LIDAR. In general, the resolution of the core LIDAR is about 12 cm and not sufficient to resolve properly the pedestal but tends to overestimate its width. Therefore, the cut-off radii of the reflectometer channels are probably even closer to the separatrix, which EFIT predicts to be at R = 3.86m (with an uncertainty of ~1cm) for this case. It is difficult to give on this basis an accurate estimate of the radial extent of WB modes with respect to the width of the transport barrier, but it is certain that WB modes are located at the plasma edge, occuring at least at pedestal radii but possibly extending further inwards into the plasma. One can further see from figure 2 that WB modes show no radial phase inversions but have twisting parity, hence they are not magnetic islands.

In general, WB modes only occur in H-Mode, where they are a very common phenomenon. They have never been observed in L-Mode, indicating that their existence is intrinsically linked to the existence of a pedestal. It is worth taking a closer look into what concerns the WB mode propagation. In general, measured mode frequencies have contributions from both plasma rotation and diamagnetic drifts. When the toroidal field and plasma current have the same sign, neglecting toroidal components of the diamagnetic drifts and taking for simplicity circular geometry, the measured frequency for modes with $m - nq = 0$ is given by [6]

$$f_{meas} \approx n \frac{\upsilon_\phi(r)}{2\pi R_0} + m \frac{\upsilon_\theta(r)}{2\pi r} - f_{*i}(r) + f_{prop}(r) \qquad (1)$$

where υ_ϕ and υ_θ are the toridal and poloidal rotation velocity, respectively, n/m are the toroidal/poloidal mode numbers and

$$f_{*i}(r) = \frac{m}{2\pi r}\,\frac{p'_i(r)}{en_e(r)B_\phi} \qquad (2)$$

is the ion diamagnetic frequency. When comparing with experimental data, instead of f*i the electron diamagnetic frequency will be used as reference, which is a better diagnosed quantity (when collisionality is high enough $f_{*\mathrm{i}}(r) \approx f_{*\mathrm{e}}(r)$ gives a reasonable approximation). At pedestal radii the diamagnetic drift gives an important contribution to the final mode propagation frequency due to the strong pedestal gradient and the lower toroidal plasma rotation at the edge. The last term in (1) is in most cases proportional to m and comes from inclusion of diamagnetic effects in the calculation of the dispersion relation for instabilities, yielding a finite mode propagation frequency f_{prop} in the frame where $\mathrm{E_r} = 0$ 3 (see e.g. [8] and references therein). Within this frame ideal MHD modes generally propagate in the direction of the ion diamagnetic drift (this applies, for example, to the type-I ELM precursors), while for other modes the direction of propagation depends on the particular type of mode (e.g. for tearing modes the dispersion relation shows that they propagate in the direction of the electron diamagnetic drift). For WB modes f_{prop} is not known, but experimentally they are observed to rotate opposite to the type-I ELM precursors in spite of being observed at similar radii. This indicates that for WB modes f_{prop} has opposite sign compared to the ELM precursors, and according to theory this implies that WB modes are not ideal MHD modes (and, in particular, that WB modes are not ideal ballooning or kink instabilities). Furthermore, as WB modes rotate opposite to the toroidal plasma rotation, the gradually increasing WB frequency between ELMs cannot be explained in terms of toroidal plasma acceleration. Instead, the characteristic frequency evolution of WB bands between ELMs (figure 1) can be explained in terms of the diamagnetic drift frequency increasing due to the gradual pedestal recovery, or in terms of gradual spin-up of poloidal plasma rotation at the barrier (provided, of course, it goes in the direction of the electron diamagnetic drift). As $f_{*\mathrm{e}}(r) \sim p'_{\mathrm{e}}(r)/n(r) \sim T_e^{ped}/\Delta_{ped}$ (where Δ_{ped} is the pedestal width and T_e^{ped} is the electron temperature at the top of the pedestal), T_e^{ped} may be used as a reference to measure relative changes in the magnitude of the diamagnetic drift. Experimentally, it is observed that there is a close relationship between the evolution of the WB frequency and that of T_e^{ped}. Figure 3 shows a comparative plot for the frequency evolution of WB bands and the evolution of T_e^{ped}, showing a good qualitative agreement in the evolution of both quantities. This coupling of WB frequency and T_e^{ped} is a very general observation made (a further example is shown in figure 14), and indicates that diamagnetic effects give an important contribution (probably the dominant one) to the finally measured WB mode frequencies. It is unclear to what extent poloidal plasma rotation at the edge might give a further contribution, in addition to the diamagnetic drift. Its measurement is difficult because the magnitude of υ_θ and the noise level of the CX diagnostic turn out to be comparable. Recent CX measurements [9] indicate that at JET the edge poloidal rotation speed of impurity ions may be on the order of 10-15 km/s in the direction of the electron diamagnetic drift and thus could become important. On the other hand, neoclassical theory predicts that at the tokamak edge the

impurity poloidal rotation speed can be quite different from the primary ion poloidal rotation speed [10]. As an additional difficulty, neoclassical theory also predicts the poloidal rotation to be coupled to the ion diamagnetic drift [10, 11] , and therefore both quantities might evolve together.

Equation (1) can be used to obtain a rough estimate for the *m*-numbers of the WB modes and check for consistency with other measurements. Assuming the third term to give the only dominant contribution to the final mode propagation frequency and taking $f_{*\mathrm{i}}(r) \approx T_i^{ped}/2\pi r e \Delta_{ped} B_\phi$) from experiment yields for the WB bands of figure 1 $m \approx 8n$ (for comparison, q_{95} is 3.7). If one additionally takes into account toroidal and poloidal rotation and uses for v_θ the neoclassical prediction, $m \approx 9n$ is obtained instead. For modes propagating in the direction of the electron diamagnetic drift f_{prop} will reduce *m* (e.g. for $f_{prop} \sim f_{*e}$ gives $m \approx 4$ to $5n$). The *m*-numbers obtained in this way are therefore consistent with modes located at the plasma boundary.

The amplitude of WB modes is not constant but shows a continuously bursting behaviour. This can be generally observed in spectrograms or *n*-number spectra like figure 1, where the individual WB bands are seen to be composed of intermittent pulsations rather than a continuous mode. Figure 4 gives a more quantitative picture, where the WB mode displacements measured by the edge reflectometer are shown as a function of time, averaged over $R = 3.75$ to 3.85m for the discharge of figure 2. The displacements vary continously, and are small, in the sub-milimeter range. The error bars for the measurements are included, showing that the changes in displacement magnitude are not due to noise. WB modes are difficult to analyse through ECE because the noise of the ECE channels turns out to be of the same order as the WB induced fluctuations. However, assuming that the real noise of the ECE channels is given by the thermal noise, which is determined by the pre- and postdetection bandwidth, an upper bound for the displacements associated with WB modes of roughly 1mm is obtained, which is compatible with the reflectometry results.

In general, WB bands have a rather broad and diffuse spectral extent that is often hardly observed above the background noise level in standard ELMy-H discharges, making it difficult, or sometimes even impossible, to quantify WB mode amplitudes in terms of individual power spectra. Normally, the best way to accomplish this is by using spectrograms with colourmaps chosen to change colour only in a narrow range of amplitudes around that of the WB modes. When analysing WB modes with magnetics spectrograms it is further important to correct for the frequency dependence of the measured mode amplitudes. As an example, figure 5 shows a magnetics spectrogram for a standard type-I ELMy-H discharge showing a time window comprising six type-I ELMs together with the inner and outer divertor D_α signal. The spectrogram shows that the WB modes are strongest in the time interval prior to the fourth ELM, have intermediate strength prior to the first, third and fifth ELMs, and are comparatively weak in the intervals prior to the second and the sixth ELMs. One can further see that the WB mode strength correlates well with the time Δt_{ELM} between two consecutive ELMs, with increased Δt_{ELM} occurring when the WB modes are strong. This again is a general observation. A priori, the causality of events is not clear at this stage, that is, it is not clear whether the WB modes do reach higher amplitudes in the longer inter-ELM intervals because the ELM interrupts their growing

at a later time, or whether strong WB mode activity causes a delay of the ELM crash. This issue of the causality of events is resolved by the Langmuir probe data. On the
D_α-signals fast spiky inter-ELM activity is observed, predominantly in the inner divertor, whose strength also correlates well with the WB mode strength, suggesting that the WB bursts cause an intermittent loss of particles at the plasma edge. This is confirmed by the Langmuir probes. In figure 6 the ion saturation current measured by four probes is shown for the same time interval, together with their relative distance to the high/low field side strike point coordinates. In particular, the spiky WB-related activity is mainly detected by the probes in the inner divertor, consistent with the D_α data, while on the low field side it is hard to observe. A closer look into the associated fluxes of particle and energy (figure 7) reveals that the WB-related activity is seen to be in phase by probes on both sides of the inner strike point. This observation confirms the existence of a true flux of particles and energy continuously expelled in short bursts, and excludes the signal fluctuations originating from fast movements of the strike point because in the latter case the signals of probes positioned below and above the strike point would be in counter-phase. Therefore, WB modes do lead to a continuous loss of energy and particles in inter-ELM periods, and increasing WB mode activity causes a delay in the onset of the next type-I ELM. WB modes show a characteristic behaviour in gas puff scans. Figure 8 shows a series of discharges with different levels of gas fuelling. With increasing gas puff the spectral distribution of WB modes becomes narrower and evolves towards lower frequencies, which is consistent with the gradually lowered edge temperature. When fuelling levels are low, the individual WB bands are usually well separated from each other in frequency and thus clearly discernable in spectrograms. With increasing fuelling the WB band frequencies tend to become closer to each other, and at sufficiently high fuelling rates they might merge into a broader band of WB activity where the individual WB bands composing it might be difficult to discern anymore. At high gas rates the WB activity usually tends to occur only around ~10 to 40 kHz. Furthermore, in JET discharges with strong gas puffing the edge temperature in-between ELMs normally saturates well before the next ELM crash and, linked to this, the WB frequency remains constant.

3. WB MODES AND TYPE-II ELMS

The “normal” ELM frequency behaviour observed in low triangularity discharges is that the type-I ELM frequency increases with increasing level of gas puffing. Three effects contribute to this behaviour: First, the pressure at the top of the pedestal (and therefore the pedestal energy content) is observed to decrease with increasing density. Therefore, at fixed input power, less time is needed for the pedestal to reach a critical gradient. Second, the energy loss per ELM relative to the pedestal energy content is observed to decrease with density. Third, the recovery of pedestal density between ELMs is observed to improve (the simplest explanation is the increased gas fuelling, but changes in inter-ELM transport might play a role as well). Discharges at high triangularity (δ ~0.5) show a clear deviation from the standard ELM behaviour, with the ELM frequency decreasing for the higher fuelling rates [12–14], as shown in figure 9. In spite of the lowered ELM frequency, the

energy loss per ELM does not increase in these cases [12]. Instead, simple power balance considerations demonstrate that the lowered ELM frequency originates from increased inter-ELM losses [15]. The anomalous ELM frequency behaviour is accompanied by broadband MHD activity around 30 kHz propagating in the direction of the electron diamagnetic drift and a characteristic grassy signature on the inter-ELM divertor D_α [16]. The similarity of the observations with the type-II ELM regime observed in ASDEX-U [17] justified the identification of the anomalous ELM regime observed at JET as a mixed type-I/type-II ELM regime [15].

Figure 10 shows the parameter evolution of a typical type-I/type-II ELM discharge at JET. The presence of a mixed ELM regime during the gas puff phase is recognisable through the lowered type-I ELM frequency compared to after fuelling switch off. Figure 11 gives an overview of the MHD activity, and in particular of the WB activity, observed at times with and without the gas puffing. (The gas puffing has been switched off at ~22.5s.) The WB mode frequencies behave in the expected way, as described in section 2: During the gas puff the WB modes tend to keep constant frequency between ELMs and occur only around 10 – 40 kHz. After switching off the fuelling the WB bands evolve towards higher frequencies, covering a wider spectral range. The remarkable point is that it is the enhanced activity seen at 10 – 40 kHz during the gas puff phase that has been associated with the type-I/type-II ELM regime occurence [16]. It is evident that this are WB modes.

In fact, there is a clear difference in WB amplitude behaviour during gas scans in low and high triangularity discharges. Figure 12 shows magnetics spectrograms for two pairs of discharges. In order to allow for comparison, the mapping of amplitudes to colours is the same for each pair of discharges. In the case of low triangularity (figure 12(a),(b); 2.4 T, 2.4 MA, 15 MW NBI), gas puffing weakens the WB activity, while in high triangularity discharges (figure 12(c),(d); 2.7 T, 2.5 MA, 15 MW NBI) the WB activity is clearly enhanced with gas fuelling. The enhancement of WB modes through gas fuelling at high triangularity and the associated increase of inter-ELM losses can therefore explain the ELM frequency anomaly and the occurence of a mixed type-I/type-II ELM regime at JET. According to this, the WB modes themselves are the type-II ELMs observed at JET, but it has to be emphasized that WB modes are also present in regimes regarded as pure type-I ELM regimes. It has been shown in the previous section that WB modes regulate the pedestal dynamics through inter-ELM losses also in the latter regime.

4. WB MODES AND TYPE-I ELM PRECURSORS

The properties of a class of low frequency type-I ELM precursors commonly observed at JET have been presented in considerable detail in [6]. The precursors occur at pedestal radii, like the WB modes, and the observed toroidal mode numbers range from $n = 1$ to ~14, Precursors with low n-numbers 1 – 3 have been identified as external kinks, while with increasing n-numbers the precursors are believed to be peeling-ballooning modes. Longer-lived precursors can be quite active in the sense they are often observed to grow and shrink repeatedly before an ELM with no evident cause. In figure 13 an example is shown where, in addition to the WB modes (again in blue), a yellow

coloured (n = +4) type-I ELM precursor starting long time before the type-I ELM crash occurs around 15 kHz (the type-I ELM happens at 21.68s). At first sight, both the WB modes and the precursor coexist over roughly 150ms, but a closer look (zoom view of figure 13) reveals that the precursor continuously appears and disappears. The remarkable feature is however that at times where the precursor occurs the WB activity vanishes. Therefore, the precursors are found to interact with the WB modes, with this interaction being mutually exclusive, i.e. at precursor appearance the WB modes are immediately weakened or even inhibited. The possibility that a weakening of the WB modes allows the ELM precursors to grow can be excluded by discharges ([5], figure 2) in which the WB modes do weaken but the ELM precursors do not immediately start to grow. Thus, the causality appears to be that the growth of the ELM precursor weakens the WB modes, and not the reverse.

In general, the order of events observed is that after the previous ELM crash first the WB modes reappear and later on usually one or more type-I ELM precursors set in, weakening the WB modes. In addition, the frequency of the eventually remaining WB modes is observed to increase with the precursor onset. This is best discerned if the WB frequency reached a steady value prior to the precursor appearance and an example of this is shown in figure 14a. In the time interval shown a diffuse WB band (light blue) around 35 kHz keeps more or less constant frequency over ~150ms, but, with the appearance of an ELM precursor at 16.88s (dark red mode at 5 – 10kHz, $n = 9 - 10$), the WB frequency starts to increase until it is finally interrupted by the ELM at 16.93 s. At this point it is worth recalling from section 2 that a coupling exists between the WB frequency and electron temperature evolution measured near the pedestal top. Together with the mode number spectrum the corresponding traces of edge temperature and line-averaged edge density are shown, obtained through ECE and interferometry, respectively. The temperature evolution resembles the WB frequency, and in particular the pedestal temperature begins to rise with the ELM precursor appearance (highlighted by the arrow). The pedestal temperature increase does not originate from a simultaneous decrease in pedestal density. Instead, the density remains increasing and seems not be be greatly affected. Hence, the onset of a type-I ELM precursor and the subsequent weakening of WB modes accelerates the pressure build-up at the transport barrier, finally allowing for or at least advancing the ELM event.

It has to be underlined that this pattern is not restricted to the above example but is a robust phenomenon that has been observed repeatedly in JET discharges. Without going further, figure 15 shows the magnetics spectrogram and fast ECE signals corresponding to the spectrum of n-numbers used for the introductory example of figure 1. As seen on the spectrogram, the longer-lived (lasting ~25ms) precursors around 18 kHz prior to the second and third ELM inhibit a WB band at 25 kHz. The precursor oscillations are detected on the fast ECE channel measuring 2 cms inside the separatrix (in the pedestal region of strong gradients), while on the channels measuring 4 and 5cms inside the separatrix (near the pedestal top) one can observe a slight but still discernable increase in the slope of the edge temperature build-up when the precursors are active. Prior to the first ELM a much

shorter- lived (~1.5ms) precursor existed. Due to its shortness that precursor could not affect the evolution of the pedestal build-up significantly. The case of short precursors will be further discussed in section 5.

A general consequence of the above observations is that, in contrast to what one would expect a priori, the onset of ELM precursor modes commonly does not lead to an overall pedestal (and thus confinement) degradation, because any increase in transport associated with the ELM precursors is overcompensated by the WB mode suppression. Only ELM precursors with extraordinary large amplitude, like the low-ones that were observed in some hot-ion H-Mode discharges [18], have been seen to deteriorate the discharge performance.

Some rather exceptional cases showed that ELM precursors are not the only possible source of WB mode suppression. WB weakening with a large sawtooth has been observed in a hot-ion H-Mode discharge (the example is discussed in detail in [5], figures 2 and 3). In that case a set of WB bands with large amplitude keeps the edge temperature constant over 400ms. Then, with the sawtooth heat pulse reaching the plasma edge (leading to a sudden increase in edge temperature), the WB modes become weaker, the edge temperature begins to rise again and 15ms later the hot-ion phase ends with the appearance of an $n = 1$ ELM precursor (external kink) and the subsequent ELM. Under normal circumstances, sawteeth are not seen to affect WB amplitudes (this might require particularly large sawteeth or features linked to the hot-ion scenario). Furthermore, some cases have been found where the WB modes become stabilised "spontaneously" in the middle of an inter-ELM period with no evident cause, in particular with no precursors having been detected.

5. WB MODES AND THE PEELING-BALLOONING CYCLE

The peeling-ballooning cycle [4] represents a model for type-I ELMs that has gained wide acceptance and constitutes a promising candidate for the understanding of ELMs. It is worth briefly reviewing the order of events predicted by this cycle, which is conceptually depicted in figure 16: Just after the previous ELM crash the plasma edge resides in a state of low pressure and low edge current (lower left corner in diagram). Heating builds up the pedestal pressure gradient on a relatively fast time scale until the ideal ballooning limit is reached, where, according to the model, it is held. The peeling-ballooning model assumes that the ideal ballooning instability is a benign instability that does not induce a violent event but rather limits the operational space in a smooth way. In a further step, with the edge current gradually building up on a slower (resistive) timescale, the pedestal state moves towards the upper right corner of the stability diagram. The ELM is finally triggered when the peeling stability boundary is crossed, where the onset of peeling modes causes a further degradation in confinement and therefore a further destabilization of the peeling modes.

Comparison with the experimental observations made on JET shows some disagreement with the predictions of the peeling-ballooning cycle:

At sufficiently low edge collisionality ($\upsilon_{*e} \lesssim 0.3$) ELMs are regularly preceded by external kinks (low-n ELM precursors). The kink modes start typically 10-100 ms before the ELM [6]. Hence, in

that case the kink stability limit is reached well in advance of the ELM event. In addition, the precursor growth rate is generally not seen to increase significantly prior to the ELM. This suggests that the external kinks do not finally trigger the ELM.

The kink-limit is probably reached well before the ELM, also when higher precursors are observed. They commonly precede ELMs in discharges with low to moderate collisionality (roughly $0.3 \lesssim (\upsilon_{*e} \lesssim 0.2$, but are no longer observed in discharges with strong gas puffing, where according to modelling results the high collisionality leads to a significant reduction of the edge current and keeps the pedestal away from the kink-limit [19]. Hence, higher-*n* precursors do probably become destabilized at the kink limit, or near the top right corner in the stability triangle (consistent with being peeling-ballooning modes, as pointed out in [6]). Higher-*n* precursors are again observed to start well before the ELM (~1 – 50ms), and there is no increase in their growth rate prior to the ELM which suggests that they do not trigger it. The peeling-ballooning model does not take into account the physics of WB modes, which have been shown to play a fundamental role in the pedestal dynamics. Therefore, a modified version of the peeling-ballooning cycle that takes them into account and is consistent with the experimental observations is proposed. The individual steps are conceptually depicted in figure 17, where the WB unstable region has been shaded. Its precise shape is not known but from the observation that WB modes reappear soon after the previous ELM crash, one must conclude that they can become unstable at relatively low pedestal pressure (far below the ideal ballooning limit), and low edge current density. Starting in step 1 from a state of low pressure gradient and low edge current after the previous ELM crash, the pedestal pressure initially builds up unperturbed. Then, with the onset of WB modes and the associated increase in inter-ELM losses, the pressure build-up is slowed down, allowing the edge current to build up on a comparative timescale until the kink stability limit is reached. In step 2, ELM precursors become destabilised at the kink-limit (the ELM itself is not triggered at this stage, because experimentally the ELM precursors are not seen to trigger the ELM). The interaction of ELM precursors with the WB modes weakens or stabilises the WB modes, allowing for a further build-up of the pedestal pressure along or near the kink-limit. The pedestal may shortly move again into the kink-stable region, where the precursors become stabilised, but with the reappearance of WB modes the kink-limit will be reached soon again, leading to the observation of intermittently existing precursors (as in figure 13). If the pressure build-up occurs entirely within the kink-unstable region, the precursors will be continuously present. At this stage the mode numbers of the most unstable precursor modes might eventually change during the pedestal evolution, possibly leading to the occurrence of a sequence of precursors with different mode numbers or the existence of more than one precursor mode at a time (which has been reported in [6]). The ELM is finally triggered when the pedestal reaches the ideal ballooning limit (step 3), which, in contrast to the conventional model for the peeling-ballooning cycle, is now assumed to impose a hard limit. In this respect, certain theoretical works [20, 21] predict a general explosive feature of the ideal ballooning instability ("detonation") emerging from non-linear effects through the development of fine-scale substructures ("fingers"). After the crash the cycle repeats

again starting from a state of low pressure/low current. Notice that, unlike in the conventional peeling-ballooning cycle, the starting point for the new cycle is not to be located at the kink-stability boundary, because the end of the crash is determined by processes related to the nonlinear ballooning and not to the kink-instability. According to this new peeling-ballooning cycle, the ELM precursors (kink-/peeling-ballooning modes) observed on JET certainly play an important role in the cycle but are not directly involved in the ELM event itself.

The picture is not yet complete. Depending on the individual discharge conditions WB modes might be more or less effective in delaying the pressure build-up with respect to the peeling and ballooning stability limits. The three situations that can arise are depicted in figure 18.

Curve 1 corresponds to the case of relative strong WB modes, where the kink-limit is reached well before the ELM. As there is a rather large gap to the ideal ballooning limit, the ELM precursors will be observed over longer times in that case. In the case of slightly less effective WB modes, the pedestal state might reach the stability limits in the vicinity of the upper-right corner of the stability triangle (curve 2). The ELM precursors are then only short-lived, and the ELM crash occurs shortly after their appearance. This case is that most often observed in JET, where the shorter precursors last on the order of 0.5 to 2 ms, and the ELM occurs while the precursor amplitudes are still growing. An example has been shown in figures 1, 15, prior to the first ELM. Due to their shortness that precursors cannot affect significantly the evolution of the pedestal build-up through WB mode suppression, but as in the upper-right corner of the stability triangle the pedestal is already close to the ideal ballooning limit, one may expect that a local steepening of the pedestal gradient caused by the precursor oscillations themselves is sufficient to cross the ideal ballooning limit where the ELM is then triggered. Finally, the pedestal evolution given by the curve 3 in figure 18 corresponds to the case where the ideal ballooning limit is reached directly. No ELM precursors are then observed, and the ELM is directly triggered. There are at least two situations where this may occur. First, if the WB modes are rather weak, and second, if strong gas puffing is applied. As modelling calculations predict [19], the increase in edge collisionality associated with the gas puffing leads to a decrease of the edge current density, keeping the pedestal state away from the kink-limit. This is corroborated by experiment, because ELM precursors are currently not observed at JET with strong gas puffing, even in discharges at high triangularity with strong WB modes and low type-I ELM frequency (mixed type-I/type-II regime).

SUMMARY AND DISCUSSION

WB modes are a very common edge-localised instability observed in JET exclusively in the H-Mode regime, evidently linked to the existence of a pedestal. They are composed of several bands of continuously bursting magnetic fluctuation whose frequency evolution has been shown to be coupled to the evolution of the edge electron temperature measured near the top of the pedestal. Probe data has shown that WB modes regulate, or at least influence, the pedestal pressure dynamics through inter-ELM losses, which is consistent withthe observation that increasing WB mode activity

leads to lower type-I ELM frequencies. The WB mode enhancement through gas puffing at high triangularity explains the occurrence of the regime identified as mixed type-I/type-II ELM regime on JET. The characteristic broadband magnetic fluctuation observed in this regime around 30 kHz and attributed to the type-II ELMs originates from the WB modes themselves. Therefore, WB modes provide the underlying mode for JET's type-II ELMs; in other words, WB modes are the type-II ELMs, but it has to be emphasized that WB modes are also present in regimes regarded as pure type-I ELM regimes, though with smaller amplitude. There is an exclusive interaction of type-I ELM precursors with the WB modes. The appearance of type-I ELM precursors weakens or even inhibits the WB modes, accelerating the pressure build-up of the pedestal followed by the ELM event. A modified version of the peeling-ballooning cycle that includes the WB physics has been proposed. It predicts the type-I ELMs to be triggered at the ideal ballooning limit rather than the kink-/peeling-boundary, and is therefore consistent with the experimental observation that the ELM precursors (kink-modes/peeling-ballooning modes) are not seen to trigger the ELM on JET.

Several open questions remain. Certainly, the most relevant one concerns the nature of the WB modes, which remains an unresolved issue. WB modes have twisting (not tearing) parity, so magnetic islands can be excluded. The list of candidates can be further reduced by the identification of WB driving or stabilising forces. Current driven modes can be excluded from the observed WB mode enhancement through gas puffing (at high triangularity). For current driven modes a weakening would have been expected due to the reduced edge current density associated with the high edge collisionality. The case mentioned in section 4 where WB modes become stabilised by a large sawtooth serves to exclude ideal pressure driven modes. In that case, the sawtooth heat pulse causes a sudden increase of the edge temperature while the edge density remains nearly unaffected. Therefore, the WB suppression coincides with a sudden increase in the overall edge pressure, which is difficult to justify in terms of an ideal pressure driven mode. Nevertheless, the increase in edge temperature implies a decrease in edge resistivity, and thus resistive pressure driven modes cannot be excluded. Resistive ballooning modes (RBMs) have been regarded as a possible candidate to explain the WB modes in [5], where several arguments in favour or against this are discussed in detail. In particular, RBMs have twisting parity [22] and certain branches are expected to propagate in the direction of the electron diamagnetic drift [23], like the WB modes, but on the other hand the n-numbers observed in the experiment are rather low. A ballooning character of the WB modes was inferred in [5] from the observed amplitude asymmetry measured by coils on the inboard and outboard side of the plasma. However, recent modelling calculations performed with MISHKA [24] in real JET geometry have shown that mode-induced field perturbations are subject to higher damping on the HFS than on the LFS, and that this may introduce a strong inboard-outboard asymmetry in the coil-measured amplitudes even if the mode itself does not have ballooning character (more details are given in [6]). Therefore, the question whether WB modes have ballooning character or not should be left open.

Kelvin-Helmholtz (KH) instabilities [25] may provide an alternative explanation for the WB

modes. KH modes are driven by the shear of the parallel plasma velocity, which is expected to be large at the H-Mode barrier, while density and temperature gradients provide a stabilising effect. They are not expected to be highly localised but to have rather broad radial extent, and are not bound to a certain rational surface, that is, their m and n numbers do not have to correspond to the local value of the safety factor. Lacking an accurate measurement for the m-numbers, the latter feature could neither be established nor refuted for the WB modes. The stabilisation of WB modes by the ELM precursors could be easily explained in terms of KH, because one expects the ELM precursors to affect the rotational shear at the edge. In similar terms, the arrival of a large sawtooth heat pulse at the plasma edge should be able as well to influence the parallel velocity shear and thus possibly stabilise the WB modes. Recent calculations that take into account the stabilising effect of both the temperature and the density gradients on the KH modes, show that they propagate (in the frame where $E_r = 0$) in the direction of the electron diamagnetic drift, with a frequency f_{prop} that is a fraction of the electron diamagnetic frequency [26].

With the perspective on ITER operation and the avoidance of large transient heat-loads onto the divertor tiles the achievement of a stationary high confinement regime combined with small ELMs is certainly desirable. These conditions have been established in the type-II or 'grassy' ELM regimes of DIII-D [27], JT-60U [28] and ASDEX Upgrade [17]. On JET, this could not be achieved yet, and it is questionable whether a mere further enhancement of the WB activity will be sufficient to obtain a pure type-II ELM regime. As shown in section 4, the WB modes are potentially capable of bringing the edge temperature to saturation. However, the edge density is not greatly affected by them but keeps increasing, at least in the gas puffed discharges. This highlights a serious problem because without a constant pedestal pressure a steady state regime will not become possible. It might be that WB modes on their own are not sufficient but that additional effects concerning the edge-related MHD have to come into play. A thorough comparison from the MHD point of view of the small ELM regimes obtained in other tokamaks is likely to clarify whether these also rely on WB-like activity and whether there is a key ingredient that is missed in JET. This is intended for future work.

From the point of view of ELM and pedestal physics, it is further desirable to ascertain whether MHD activity comparable to JET's WB modes is observed in type-I ELM regimes elsewhere. Taking into account how commonly WB modes are observed on JET, one might expect them also to be present in other machines. It is unlikely that WB modes are related to the quasi-coherent mode (QCM) observed during the EDA-regime [29] of Alcator C-Mod, although there are some similarities. In particular, both modes occur at the plasma edge, rotate in the direction of the electron diamagnetic drift and lead to a continuous loss of energy and particles into the SOL [30]. There are, however, two large differences. First, the observed toroidal mode numbers of the QCM are in the range $n = 15 - 18$ [31], which is much larger than those of the WB modes. Second, WB modes are currently composed of several bands of magnetic fluctuation activity, while for the QCM it is only a single band.

As a concluding remark, any effort giving further insight into the WB mode phenomenon is

potentially capable of shedding light onto H-Mode and edge transport barrier physics. The strong decrease in transport associated with the formation of an H-Mode barrier is thought to originate from the suppression of turbulence across the pedestal. The results presented here permit one to draw already the conclusion that the pedestal transport at JET is nevertheless still determined by anomalous, not neoclassical, processes.

ACKNOWLEDGMENTS

This work has been performed under the European Fusion Development Agreement.

REFERENCES

[1]. Zohm H 1996 Plasma Phys. Control. Fusion **38** 105
[2]. Connor J W 1998 Plasma Phys. Control. Fusion **40** 191
[3]. Connor J W 1998 Plasma Phys. Control. Fusion **40** 531
[4]. Connor J W, Hastie R J, Wilson H R 1998 Phys. Plasmas **5** 2687
[5]. Smeulders P et al 1999 Plasma Phys. Control. Fusion **41** 1303
[6]. Perez C P et al submitted to Nucl. Fusion
[7]. JET Team (presented by Jones T T C) 1995 Plasma Phys. Control. Fusion **37** A359
[8]. White R B 1989 Theory of Tokamak Plasmas, North Holland, section 5.11
[9]. Andrew Y et al 2002 'Local Edge Parameters at the L-H Transition on JET', 44th APS Conference Annual Meeting of the Division of Plasma Physics, Orlando, USA
[10]. Kim Y B, Diamond P H, Groebner R J 1991 Phys. Fluids B **3** 2050
[11]. Hazeltine R D 1974 Phys. Fluids **17** 961
[12]. Loarte A et al 2001 Proc. 28th EPS Conf. on Controlled Fusion and Plasma Physics (Madeira, 2001) P3.005
[13]. Saibene G et al 2001 Proc. 28th EPS Conf. on Controlled Fusion and Plasma Physics (Madeira, 2001) P3.002
[14]. Loarte A et al 2002 Plasma Phys. Control. Fusion **44** 1815
[15]. Saibene G et al 2002 Plasma Phys. Control. Fusion **44** 1769
[16]. Becoulet M et al 2002 Plasma Phys. Control. Fusion **44** 103
[17]. Stober J et al 2001 Nucl. Fusion **41** 1123
[18]. Nave M F F et al 1997 Nucl. Fusion **37** 809
[19]. Parail V et al 2002 Proc. 19th IAEA Fusion Energy Conference (Lyon, 2002) IAEA-CN-94-TH/P3-08
[20]. Hurricane O A, Fong B H, Cowley S C 1997 Phys. Plasmas **4** 3565
[21]. Fong B H 1999 PhD thesis, available at http://www.asp.ucar.edu/B bhlfong/thesis.pdf
[22]. Strauss H R 1981 Phys. Fluids **24** 2004
[23]. Diamond P H et al 1985 Nucl. Fusion **28** 1116
[24]. Mikhailovskii A B et al 1997 Plasma Phys. Rep. **23** 844

[25]. D'Angelo N 1965 Phys. Fluids **8** 1748
[26]. Rogister A, Singh R in preparation
[27]. Ozeki T et al 1990 Nucl. Fusion **30** 1425
[28]. Kamada Y et al 2002 Plasma Phys. Control. Fusion **44** A279
[29]. Greenwald M et al 1997 Nucl. Fusion **37** 793
[30]. Snipes J A et al 2001 Plasma Phys. Control. Fusion **43** L23
[31]. Snipes J A et al 2002 Proc. 29th EPS Conf. on Controlled Fusion and Plasma Physics (Montreux, 2002) P1.057

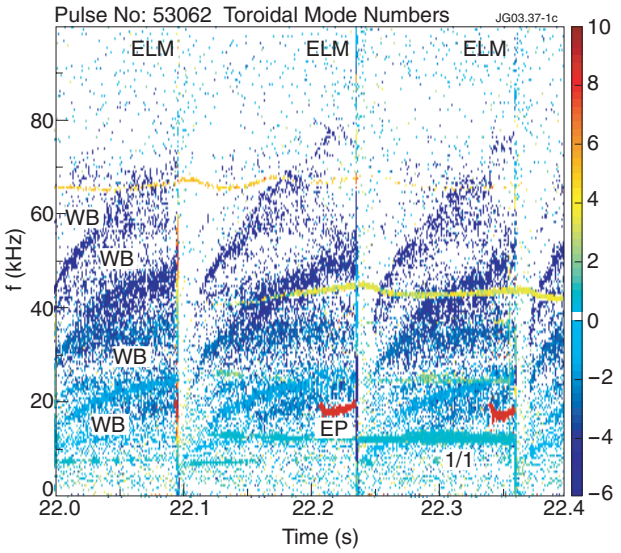

Figure 1: Spectrum of toroidal mode numbers n. Three type-I ELMs occur at 22.096s, 22.24s and 22.36s. The red coloured modes (n + 8) are type-I ELM precursors [6]. The WB modes are the multiple blue coloured broader bands propagating in the direction of the electron-diamagnetic drift (negative!-numbers).

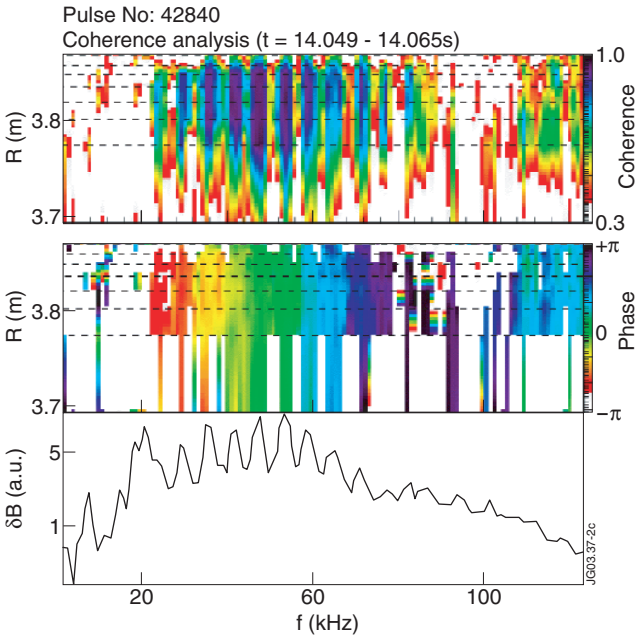

Figure 2: Coherence and phase spectra as a function of frequency and major radius R for a set of multiple WB bands (taken from [5]). The separatrix as calculated by EFIT is at R = 3.86m. The colour scales are shown at the right of each plot. The dashed lines denote the measuring radii of the reflectometer channels. The WB bands occur at ~20 – 75 kHz. The third plot shows the power spectrum of the reference Mirnov signal, where the individual WB bands are clearly visible.

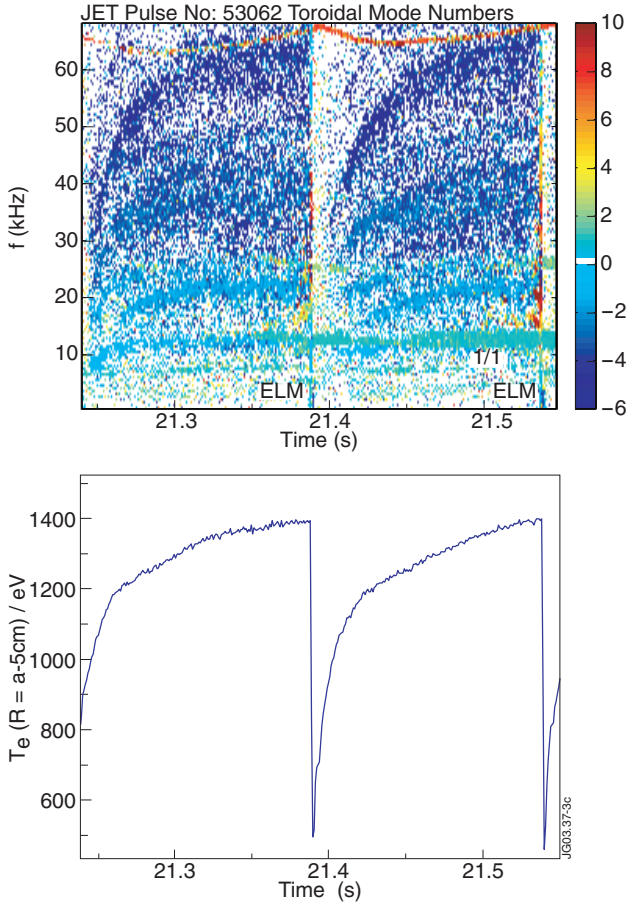

Figure 3: (a) Spectrum of toroidal mode numbers showing the WB frequency evolution and (b) electron temperature at the pedestal shoulder measured by means of ECE showing a close relationship between both quantities. In (a) the green coloured mode around 13 kHz is a sawtooth precursor.

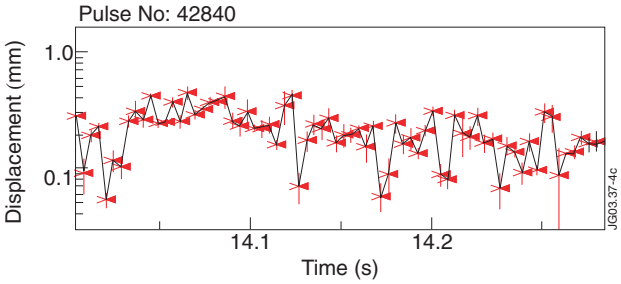

Figure 4: Displacement from n_e-fluctuations caused by WB modes. The time resolution is limited to 4 ms by the number of points required for the coherence analysis (from [5]).

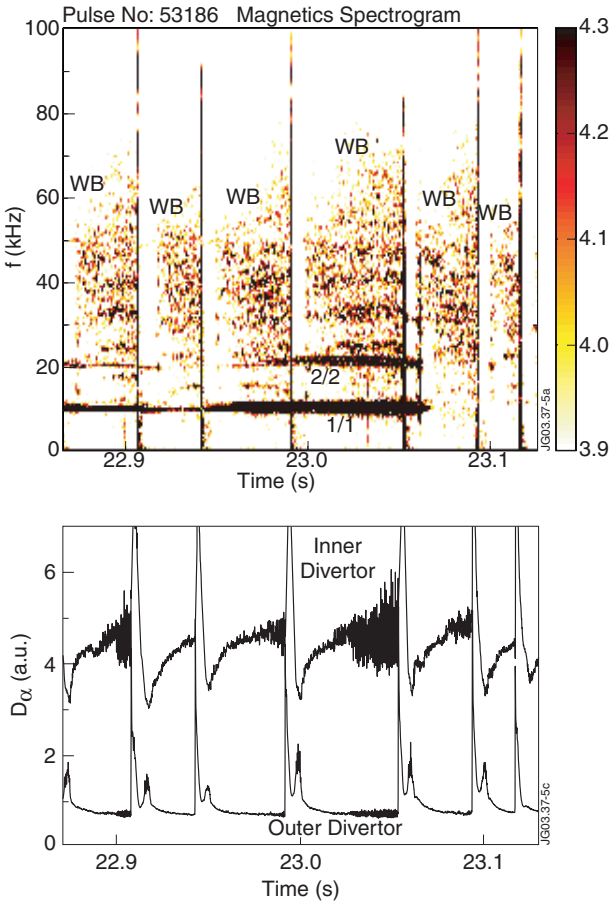

Figure 5: Magnetics spectrogram for a time interval with different levels of WB activity between ELMs, and corresponding divertor D_α signals showing fast bursting inter-ELM activity linked to the occurrence of WB modes and their amplitude. With increasing WB amplitudes the time between two consecutive ELMs increases as well.

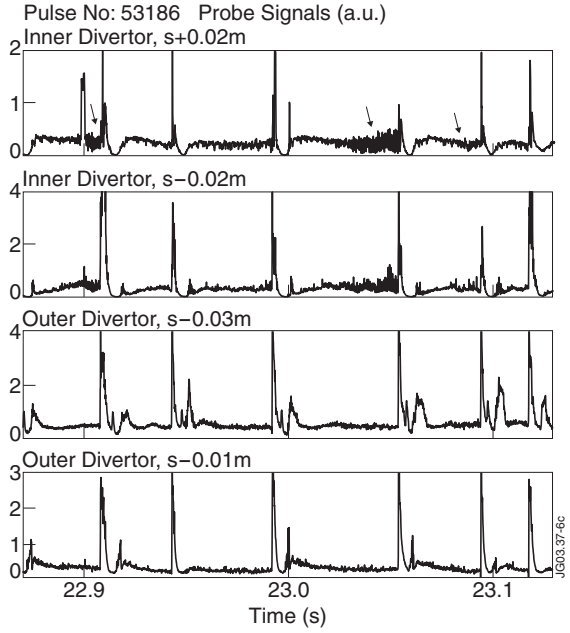

Figure 6: Ion saturation current from four Langmuir probes located in the divertor for the same time interval as figure 5, together with their distance to the high/low field side strike point coordinates (as calculated by EFIT). The arrows point at the fast WB-related inter-ELM activity.

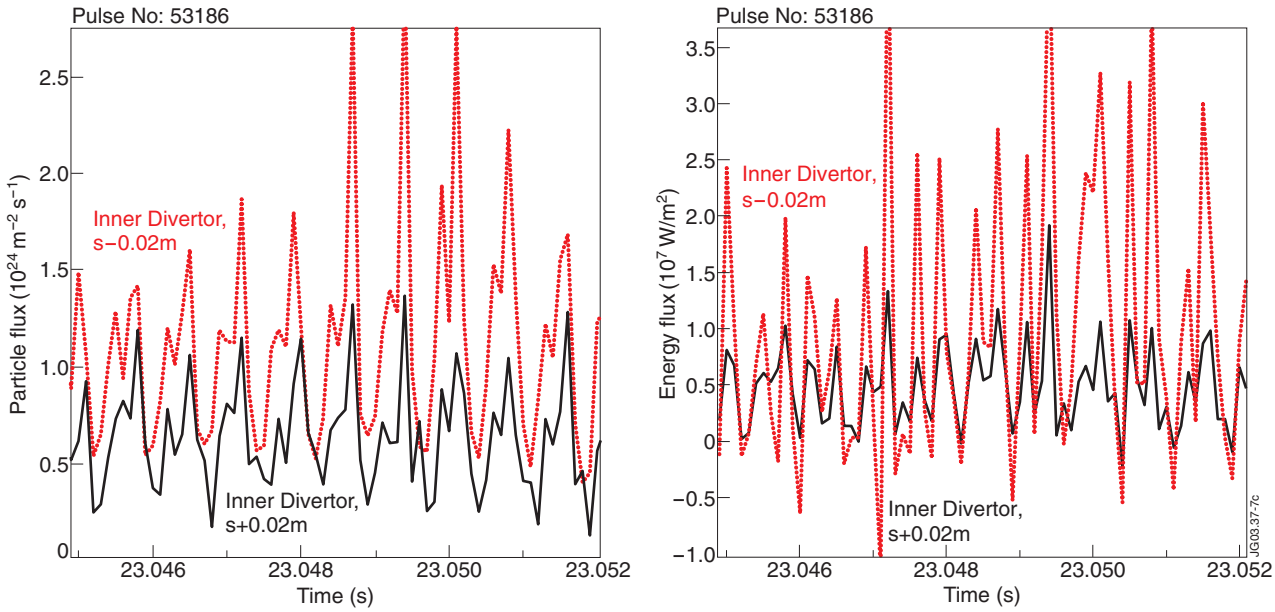

Figure 7: WB-related particle and energy flux measured by Langmuir probes on both sides of the strike point in the inner divertor. The given distance to the strike point has been calculated with EFIT. Cross-checking with the level of ion saturation current on various probes confirmed the strike point to unambiguously lie between the two probes shown. In the calculation of the energy flux, a sheath-transmission factor of 8 has been used.

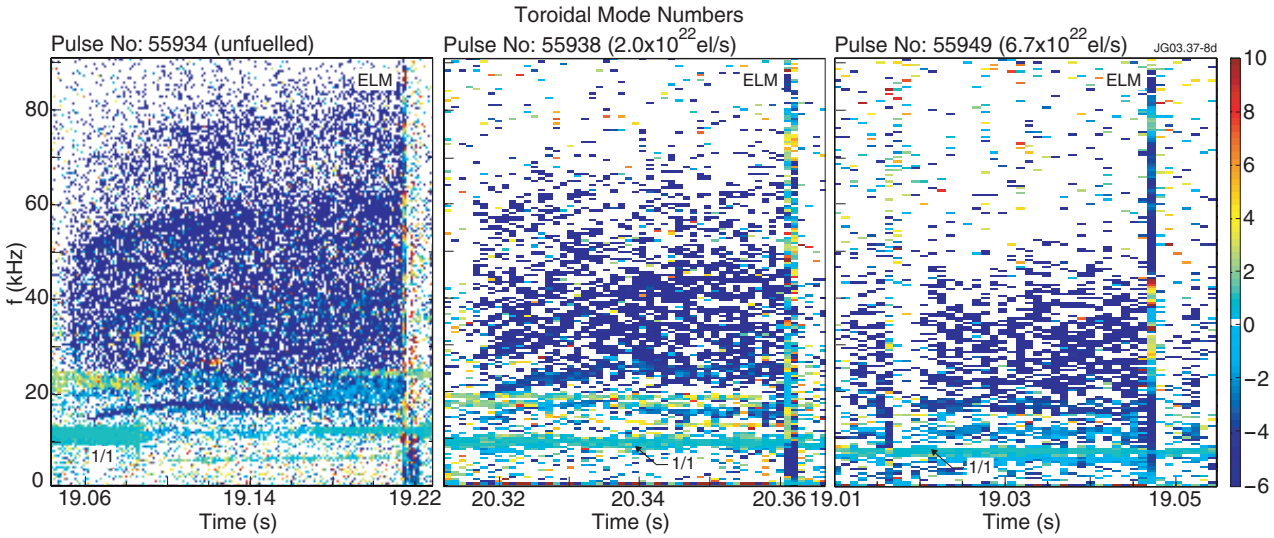

Figure 8: WB modes in a gas puff scan (DOC-configuration, low triangularity). With increasing gas fuelling (from left to right) the spectral distribution of WB modes becomes narrower and evolves towards lower frequencies. This frequency behaviour is consistent with the gradually lowered edge temperature due to the gas puffing. At high gas rates the WB bands usually tend to occur only around 10 to 40 kHz. The green-coloured modes around 10 kHz are sawtooth precursors.

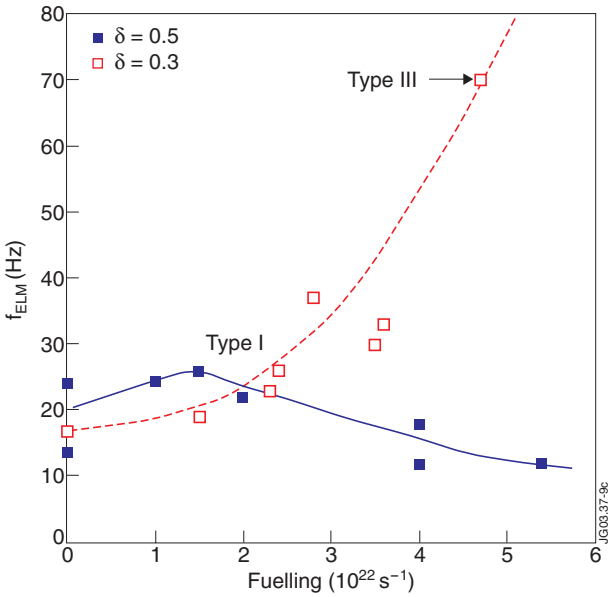

Figure 9: Behaviour of ELM frequency with increasing levels of gas fuelling for two scans performed at low ($\delta = 0.3$) and high ($\delta = 0.5$) plasma triangularity, respectively (from [14]). For discharges at high triangularity the ELM frequency decreases for sufficiently high fuelling rates, showing a clear deviation from the standard ELM frequency behaviour. This observation led to the identification of a mixed type-I/type-II ELM regime at JET.

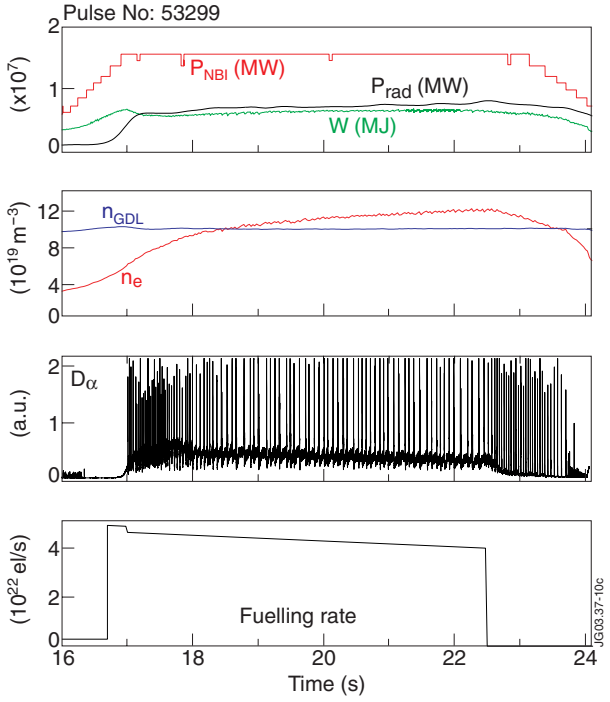

Figure 10: Parameter evolution of a typical JET discharge (2.7T, 2.5MA, $\delta = 0.5$) with mixed type-I/type-II ELM regime. Shown are (a) the NBI power, the plasma energy content W and the radiated power P_{rad}, (b) the line averaged density together with the Greenwald density limit, (c) the divertor D_α signal, where the large spikes are due to type-I ELMs, and (d) the gas fuelling rate. The presence of a mixed ELM regime during the gas puff phase is recognisable through the lowered type-I ELM frequency while gas fuelling is on.

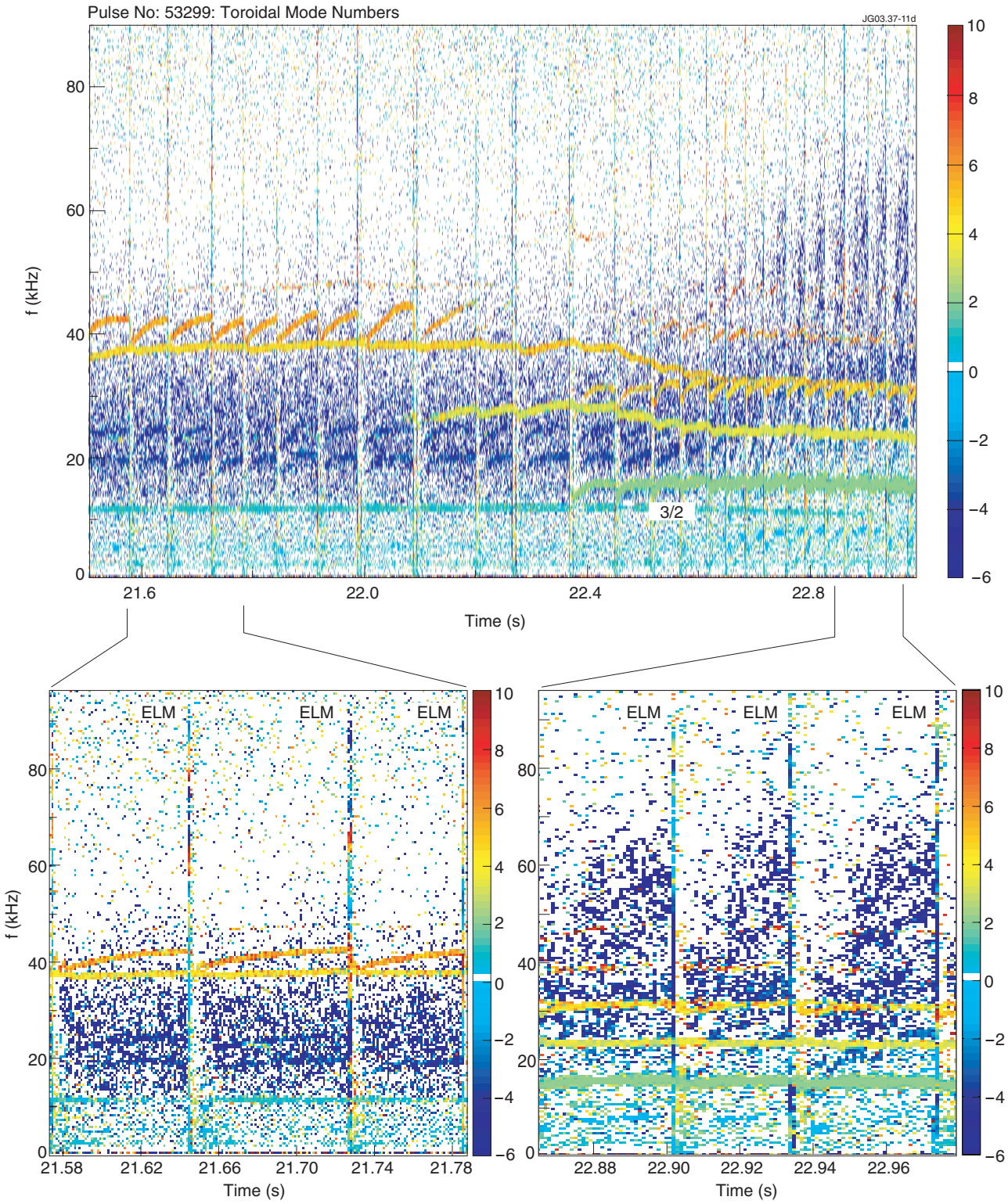

Figure 11: Spectrum of toroidal mode numbers for the same discharge as figure 10, taking closer looks into the WB activity (in blue) in mixed type-I/type-II ELM regime (during gas puffing) and in type-I ELM regime (gradually recovered after switching off the gas fuelling at ~22.5), respectively.

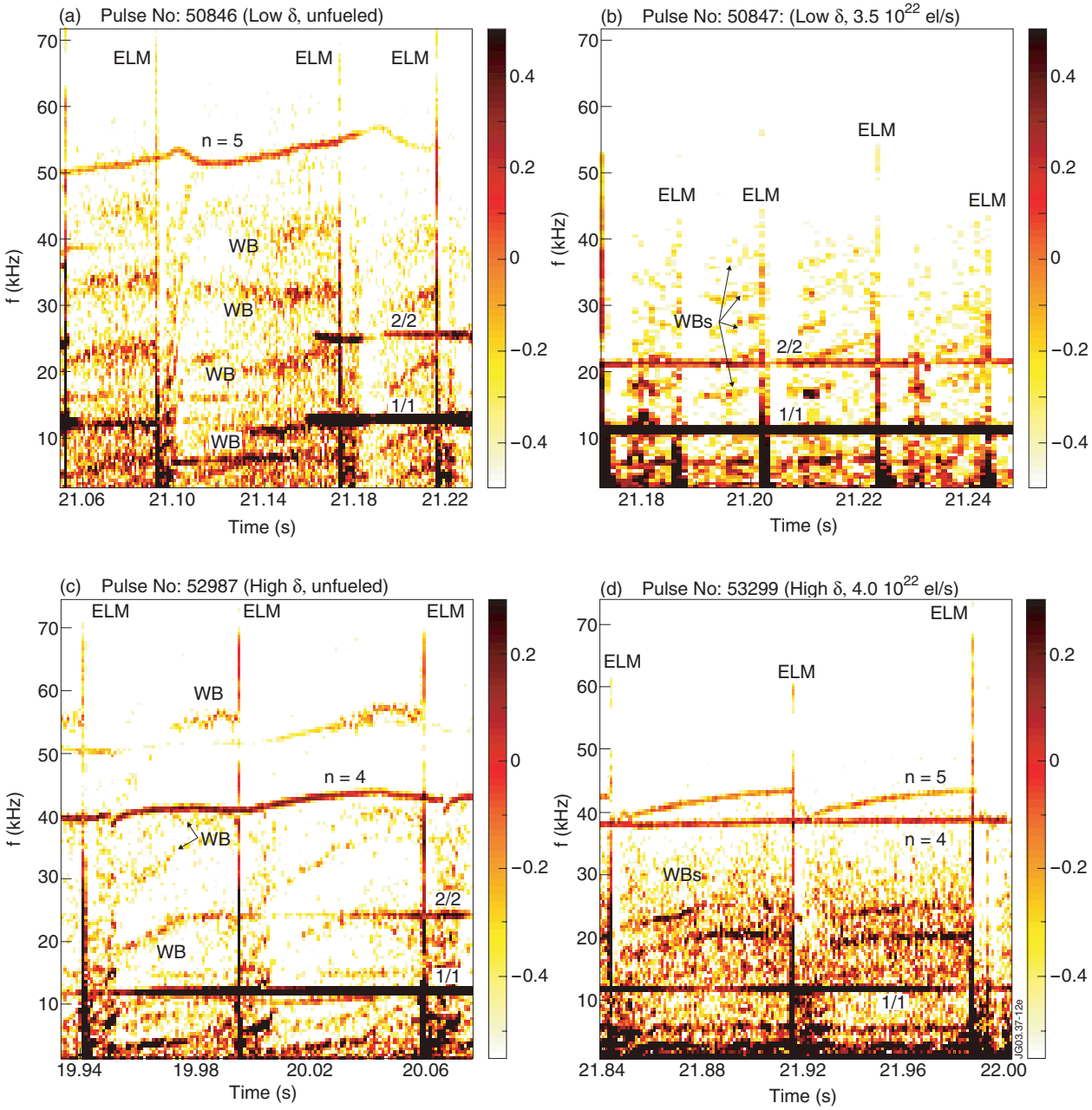

Figure 12: Magnetics spectrograms for two pairs of low ($\delta = 0.3$) and high triangularity ($\delta = 0.5$) discharges with and without strong gas fuelling. At low triangularity WB modes become weaker with fuelling, whereas at high triangularity it is the opposite case. The colourmap for the amplitudes has been kept fixed for each pair to allow for comparison.

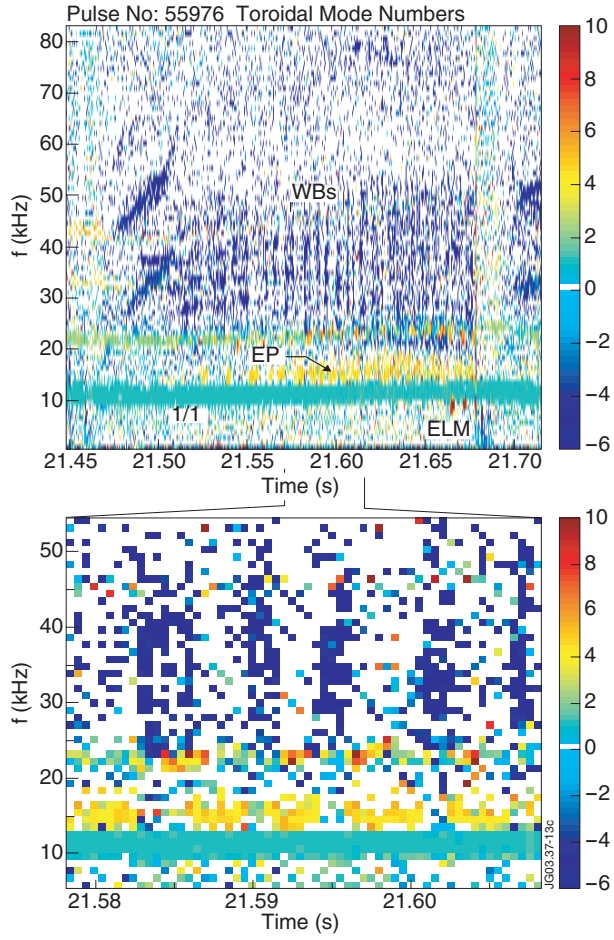

Figure 13: Spectrum of toroidal mode numbers for an inter-ELM period showing the exclusive interaction of WB modes (in blue) and an n = 4 type-I ELM precursor (yellow coloured mode around 15kHz). The type-I ELM occurs at 21.68s. The continuously present green-coloured mode at 10kHz is a sawtooth precursor. The zoom view clarifies that at times where the precursor occurs the WB modes are inhibited.

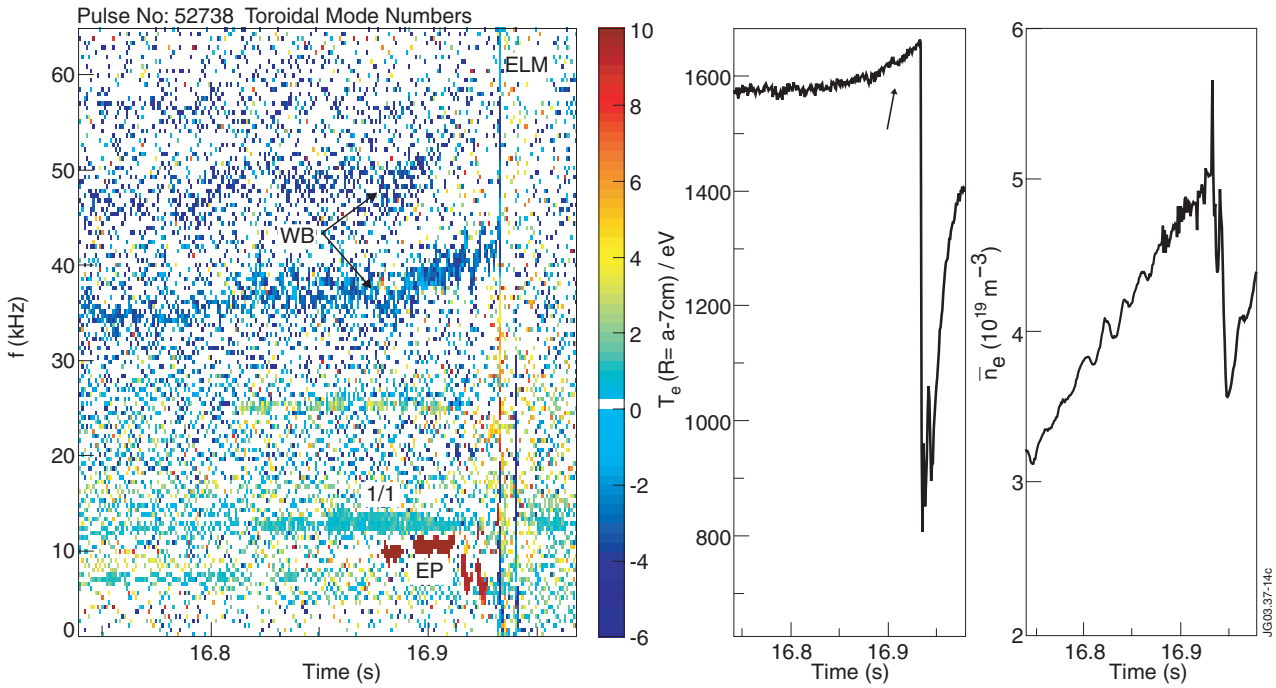

Figure 14: (a) Spectrum of toroidal mode numbers highlighting a diffuse WB band (light blue) around 35kHz. A further even more diffuse WB band occurs at 45 to 50kHz. Having had constant frequency, the appearance of a type-I ELM precursor (dark red mode at 5 – 10kHz, n = 9 – 10) at 16.88s leads to the disappearance of the WB band at 50kHz and triggers a further increase in frequency of the remaining WB band until the ELM occurs. (b) Corresponding traces of electron temperature and density measured near the top of the pedestal. The temperature evolution resembles the WB frequency, and begins to increase at precursor onset (see arrow). In contrast, the density build-up remains seemingly unaffected.

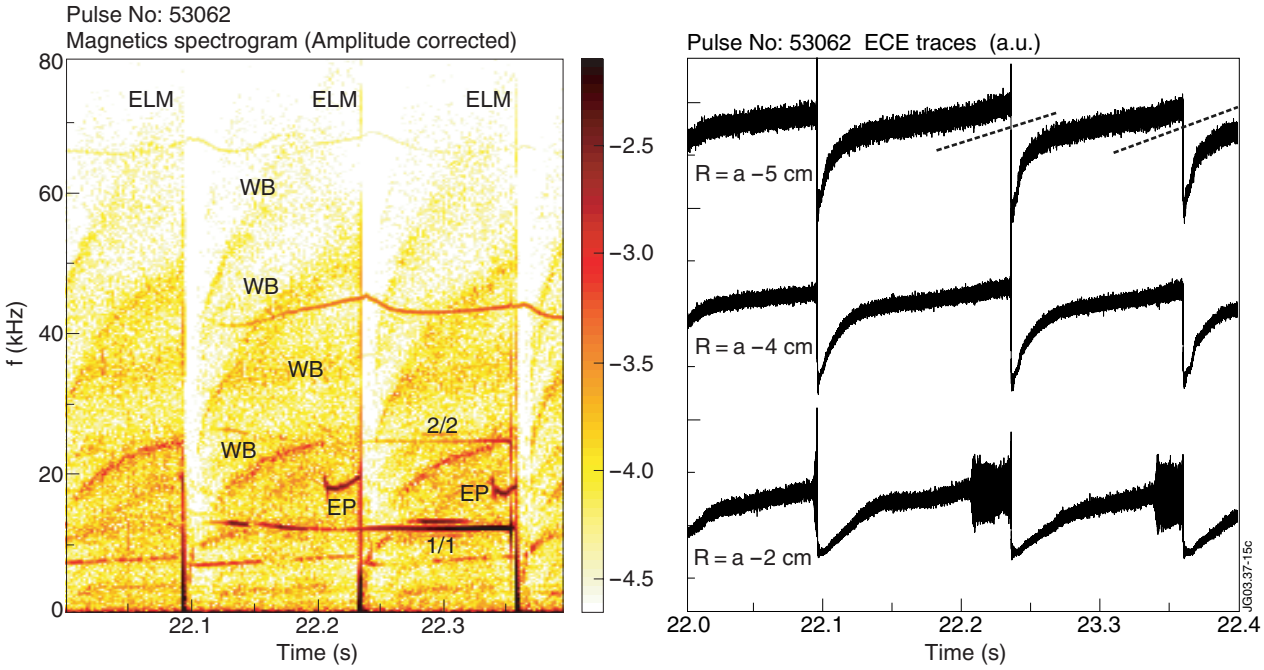

Figure 15: (a) Spectrogram of the Mirnov signal (corrected for the frequency dependence of amplitude) from a LFS coil, corresponding to the example of figure 1. The longer-lived precursors occuring prior to the second and third type-I ELMs (around 18kHz, marked by black arrows), suppress the WB band at ~25kHz (green arrow). (b) Corresponding traces of three fast ECE signals measuring close to the separatrix œ . The ELM precursor oscillations are visible on the channel measuring at 2cms inside the separatrix (in the pedestal region of strong gradients), while on the channels measuring 4 and 5 cms inside the separatrix (near the pedestal top) one can observe a slight but still discernable increase in the slope of the edge temperature build-up when the precursors are active.

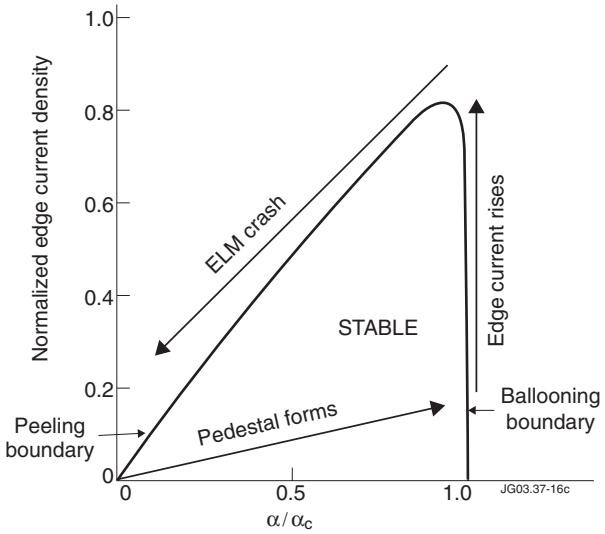

Figure 16: Stability diagramm for coupled peeling-ballooning modes in the space of normalised edge current and ballooning stability parameter showing the order of events predicted by the conventional peeling-ballooning cycle (from [3]). Just after the previous ELM crash the plasma edge resides in a state of low pressure and low edge current (lower left corner in diagramm). Heating builds up the pedestal pressure gradient on a relatively fast time scale until the ideal ballooning limit is reached, where it is limited. With the edge current gradually building up on a slower (resistive) timescale, the pedestal state moves towards the upper right corner of the stability diagramm. The ELM is finally triggered when the peeling stability boundary is crossed, where the onset of peeling modes causes a further degradation in confinement and therefore a further destabilization of the peeling modes.

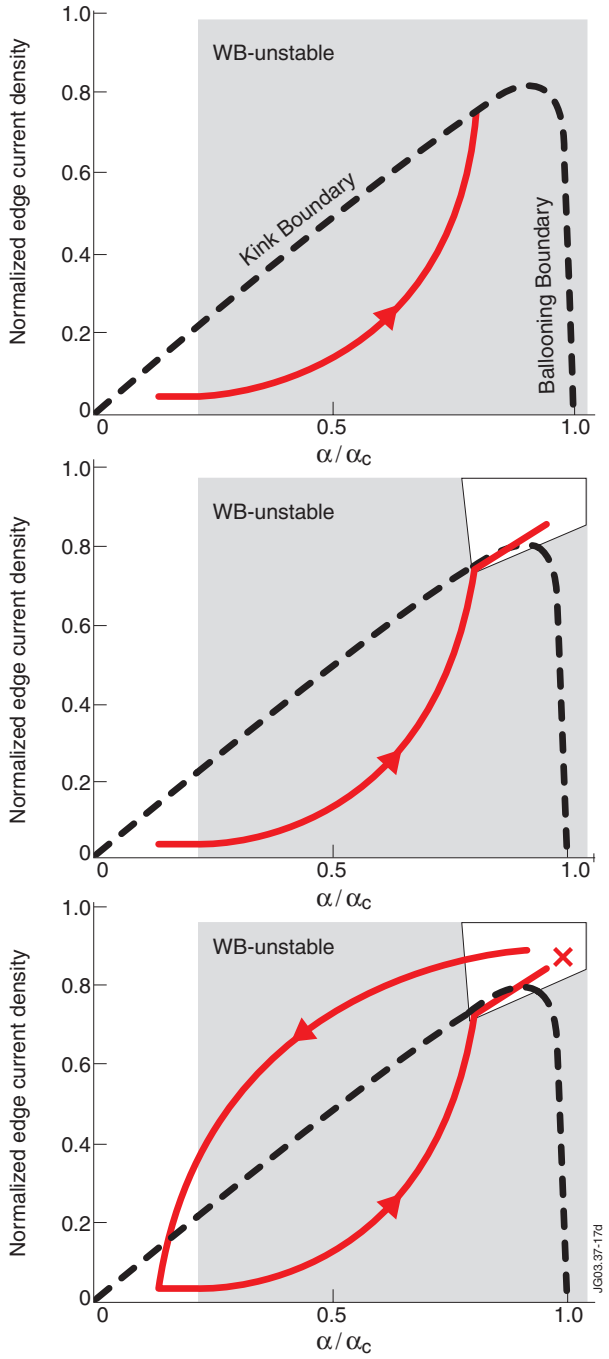

Figure 17: Individual steps of a modified peeling-ballooning cycle that takes into account the WB mode observations: (a) After the previous ELM crash the pedestal pressure initially builds up unperturbed, but, with the onset of WB modes and the associated increase in inter-ELM losses, the pressure build-up is slowed down, allowing for the edge current to build up on a comparative timescale until the kink-limit is reached. (b) ELM precursors become destabilised at the kink-limit, and their interaction with WB modes weakens or stabilises the WB modes, allowing for a further build-up of the pedestal pressure along or near the kink-limit. (c) The ELM is finally triggered at the ideal ballooning limit, which is now assumed to impose a hard limit.

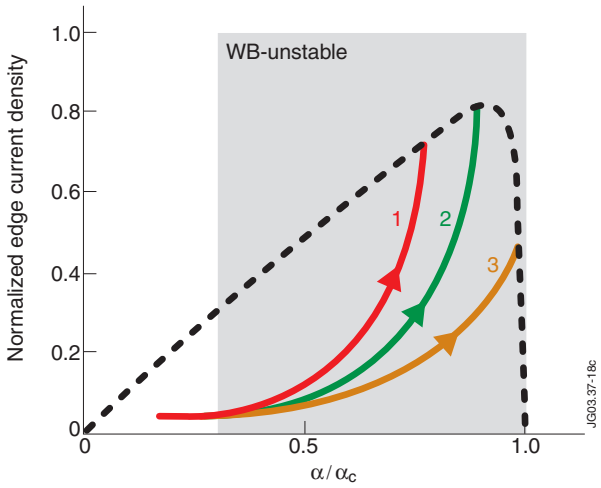

Figure 18: The three possible situations that may arise depending on the WB amplitude and discharge conditions. Curve 1 corresponds to the case of relative strong WB modes, where the kink-limit is reached well before the ELM. ELM precursors will be observed over longer times in that case. In the case of slightly less effective WB modes, the pedestal state might reach the stability limits close to the upper-right corner of the stability triangle (curve 2). The ELM occurs then shortly after the appearance of ELM precursors. The pedestal evolution given by the curve 3 corresponds to the case where the ideal ballooning limit is reached directly. No ELM precursors are then observed. The latter case may arise with rather weak WB modes, or in discharges where strong gas fuelling limits the amount of edge current.